

Manuscript prepared for The Cryosphere Discuss.  
with version 4.1 of the L<sup>A</sup>T<sub>E</sub>X class copernicus\_discussions.cls.  
Date: 1 September 2014

# Combining damage and fracture mechanics to model calving

**J. Krug<sup>1,2</sup>, J. Weiss<sup>1,2</sup>, O. Gagliardini<sup>1,2,3</sup>, and G. Durand<sup>1,2</sup>**

<sup>1</sup>CNRS, LGGE, 38041 Grenoble, France

<sup>2</sup>Univ. Grenoble Alpes, LGGE, 38041 Grenoble, France.

<sup>3</sup>Institut Universitaire de France, Paris, France

Correspondence to: J. Krug  
([jean.krug@ujf-grenoble.fr](mailto:jean.krug@ujf-grenoble.fr))

## Abstract

Calving of icebergs is a major negative component of polar ice-sheet mass balance. We present a new calving modeling framework relying on both continuum damage mechanics and linear elastic fracture mechanics. This combination accounts for both the slow sub-critical surface crevassing and fast propagation of crevasses when calving occurs. First, damage of the ice occurs over long timescales and enhances the viscous flow of ice. Then brittle fractures propagate downward, on very short timescales, considering the ice body as an elastic medium. The model is **calibrated** on Helheim Glacier, South-West Greenland, one of the well monitored, fast-flowing outlet glacier. This allows to identify sets of model parameters giving a consistent response of the model and producing a dynamic equilibrium in agreement with observed stable positions of the Helheim ice front between 1930 and today.

## 1 Introduction

Over the last decades, discharge of ice from Greenland and Antarctic ice sheets strongly increased (Shepherd et al., 2012), due to either an **intensified** submarine melting, or an increasing rate of ice calving. Recent observations have shown that the ice loss is almost equally distributed between these two sink terms despite some regional differences (Rignot et al., 2010; Depoorter et al., 2013). Ice loss by iceberg calving has been evaluated to  $1321 \pm 144$  gigatonnes per year for Antarctica in 2013 (Depoorter et al., 2013) and 357 gigatonnes per year for Greenland between 2000 and 2005 (Rignot and Kanagaratnam, 2006). These figures could become more **significant**, as the front destabilization can exert a strong positive feedback on glacier dynamics. Indeed, the abrupt collapse of the front can impact the whole glacier equilibrium, leading to both upstream thinning and acceleration by a loss of buttressing, in turn leading to a further increase in ice discharge (Gagliardini et al., 2010). The collapse of Larsen B ice shelf in 2002 (Scambos et al., 2004) or the disintegration of the floating tongue of Jakobshavn Isbrae, on the West coast of Greenland ice sheet the same year (Joughin et al., 2008a) are two examples on how perturbations near the ice front affect the upstream and even grounded portion of the adjacent glaciers.

In the sake of projecting ice sheet evolution, a deep understanding and representation of the processes occurring at the front are necessary, especially those concerning iceberg calving.

Most studies dealing with iceberg calving follow the approach proposed by Benn et al. (2007a,b). They introduced a criterion suggesting that calving occurs when a crevasse penetrates the glacier below the water level. The computation of the crevasse penetration depth is based on the work of Nye (1957), and depends on the equilibrium between longitudinal stretching (opening term) and cryostatic pressure (closing term). This so-called “crevasse-depth” criterion has been applied to individual marine-terminated glaciers of Greenland and Antarctica, allowing a successful reproduction of the front variations (Nick et al., 2010; Otero et al., 2010; Nick et al., 2013; Cook et al., 2014). Though the model of Nick et al. (2010) accounts for basal crevasse opening, which improves the capability to reproduce observed behaviour. However, this model is based on an instantaneous stress balance combined to an empirical criterion for calving. Consequently, it cannot account for the physical processes related to fracture propagation, such as the stress concentration at the tip of crevasses, and does not take into account the role of the stress history on the accumulation of damage, which may influence calving occurrence time and amplitude.

Another approach to model calving has been done using discrete elements models (Bassis and Jacobs, 2013; Åström et al., 2013). These models show interesting results in terms of calving processes and iceberg size distribution. However, the coupling of such models with finite-difference or finite-element glacier or ice-sheet models is not straightforward, and their computational cost is important.

For a few years, some authors have focused on continuum damage mechanics in order to represent both the development of micro-defects in the ice to the development of macro-scale crevasses, and their effects on the viscous behaviour of the ice while keeping a continuum approach. Initially developed for metals deformation (Kachanov, 1958), damage mechanics has recently been applied to ice dynamics to study the apparition of a single crevasse (Pralong et al., 2003; Pralong and Funk, 2005; Duddu and Waisman, 2013) or to average crevasse fields (Borstad et al., 2012). On the other hand, linear elastic fracture mechanics (van der Veen, 1998a,b) has been used to describe the rapid propagation of surface and bottom crevasses

through the ice. This approach has rarely been used in ice-sheet modeling. The reason is that a realistic representation of crevasses requires a high mesh refinement usually difficult to reach when modeling large ice masses.

Here we consider a combined approach between damage mechanics and fracture mechanics. The proposed physically-based calving model can cover both the accumulation of damage as the ice is transported through the glacier, and the critical fracture propagation in the vicinity of the calving front. The slow development of damage represents the long timescales evolution of purely viscous ice, while the use of fracture mechanics allows to consider calving events occurring at shorter timescales, for which the ice can be considered as a purely elastic medium. The description of the physics implemented is presented in Sect. 2, covering the damage initiation and its development, the fracture propagation and its arrest criterion. In Sect. 3, sensitivity tests are carried out on Helheim Glacier, and results are discussed.

## 2 Model Physics

### 2.1 Governing equations for ice flow

#### 2.1.1 Ice flow and rheology

We consider an incompressible, isothermal and gravity-driven ice-flow in which the ice exhibits a non-linear viscosity. The ice flow is ruled by the Stokes equations (*i.e.* Navier-Stokes equations without inertial term), meaning the momentum and the mass balance:

$$\operatorname{div}(\boldsymbol{\sigma}) + \rho_i \mathbf{g} = 0 \quad (1)$$

$$\operatorname{div}(\mathbf{u}) = 0 \quad (2)$$

where  $\boldsymbol{\sigma}$  represents the Cauchy stress tensor,  $\mathbf{g}$  the gravity force vector,  $\rho_i$  the density of ice and  $\mathbf{u}$  the velocity vector. The Cauchy stress tensor can be expressed as a function of the deviatoric stress tensor  $\mathbf{S}$  and the isotropic pressure  $p$ , with  $\boldsymbol{\sigma} = \mathbf{S} - p\mathbf{I}$  and  $p = -\operatorname{tr}(\boldsymbol{\sigma})/3$ . Ice rheology

is represented by a non-linear Norton-Hoff type flow law called *Glen's flow* law, which reads:

$$\mathbf{S} = 2\eta\dot{\boldsymbol{\epsilon}} \quad (3)$$

This equation links the deviatoric stress  $\mathbf{S}$  to the strain rate  $\dot{\boldsymbol{\epsilon}}$ . The effective viscosity  $\eta$  writes:

$$\eta = \frac{1}{2}(EA)^{-1/n} \mathbf{I}_{\dot{\boldsymbol{\epsilon}}_2}^{(1-n)/n} \quad (4)$$

- 5 where  $\mathbf{I}_{\dot{\boldsymbol{\epsilon}}_2}^2$  represents the square of the second invariant of the strain rate tensor,  $A$  is the fluidity parameter and  $E$  is an *enhancement factor*, usually varying between 0.58 and 5.6 for ice-flow models (Ma et al., 2010), **depending on the fabric and on the stress state**.

### 2.1.2 Boundary conditions

- The upper surface is defined as a stress-free surface. **In the coordinate system  $(x, y, z)$** , it obeys  
10 the following equation:

$$\frac{\partial z_s}{\partial t} + u_s \frac{\partial z_s}{\partial x} + v_s \frac{\partial z_s}{\partial y} - w_s = a_s \quad (5)$$

where  $z_s$  refers to the elevation of the upper surface, and  $(u_s, v_s, w_s)$  are the surface velocities. The surface mass balance  $a_s$  is prescribed as a vertical component only. As we neglect any effect of atmospheric pressure, normal and tangential stresses at the surface are zero:

$$\begin{aligned} \sigma_{nn}|_s &= 0 \\ \sigma_{nt_i}|_s &= 0 \quad (i = 1, 2) \end{aligned} \quad (6)$$

Subscripts  $n$  and  $t_i$  respectively refers to normal (pointing outward) and tangential directions.

Similar to the upper free surface, the bottom surface evolution is described by:

$$\frac{\partial z_b}{\partial t} + u_b \frac{\partial z_b}{\partial x} + v_b \frac{\partial z_b}{\partial y} - w_b = a_b \quad (6)$$

- where  $(u_b, v_b, w_b)$  are the basal velocities, and  $a_b$  represents the vertical component of the basal  
20 mass balance (melting or accretion). At the bed, the glacier can be either grounded or floating.

The grounded part of the glacier undergoes a shearing stress which is represented by a non-linear Weertman-type friction law:

$$\mathbf{u} \cdot \mathbf{n} = 0$$

$$\sigma_{nt_i}|_b = t_i \cdot (\boldsymbol{\sigma} \cdot \mathbf{n})|_b = C u_b^{m-1} u_{t_i} \quad (i = 1, 2)$$

where  $C$  and  $m = 1/3$  are respectively the friction coefficient and exponent.  $u_b$  is the norm of the sliding velocity  $\mathbf{u}_b = \mathbf{u} - (\mathbf{u} \cdot \mathbf{n}_b) \mathbf{n}_b$ , with  $\mathbf{n}_b$  the normal outward-pointing unit vector to the bedrock. Where the ice is floating the free surface is forced by an external sea pressure normal to the surface:

$$\sigma_{nn}|_b = -\rho_w g (l_w - z_b)$$

$$\sigma_{nt_i}|_b = 0 \quad (i = 1, 2)$$

where  $\rho_w$  is the water density,  $l_w$  the sea level, and  $z_b$  refers to the elevation of the bottom surface. The position between the grounded and floating part of the basal boundary, *i.e.* the grounding line, is part of the solution and computed solving a contact problem following Durand et al. (2009) and Favier et al. (2012). The inverse method described in Jay-Allemand et al. (2011) is used to infer the basal friction coefficient  $C$  by reducing the mismatch between observed and modelled surface velocities.

The ice front is defined as a third free-surface, which can also undergo melting. In analogy to the other free surfaces we get:

$$\frac{\partial x_f}{\partial t} + v_f \frac{\partial x_f}{\partial y} + w_f \frac{\partial x_f}{\partial z} - u_f = a_f \quad (7)$$

where  $(u_f, v_f, w_f)$  are the frontal velocities, and  $a_f$  characterizes the frontal mass balance. The ice front is exposed to the water pressure below sea level and is stress-free above sea level.

These Neumann conditions read:

$$\sigma_{nn}|_f = -\max(\rho_w g (l_w - z), 0)$$

$$\sigma_{nt_i}|_f = 0 \quad (i = 1, 2)$$

The list of physical and numerical parameters used in this paper is given in Tab. 1. Some boundary conditions are specific to the 2D flowline application conducted in Sect. 3, and are described in detail in Sect.3.2.

## 2.2 Continuum damage mechanics model

Continuum Damage Mechanics (CDM) was introduced by Kachanov (1958) to quantify the degradation of mechanical properties resulting from the nucleation of internal defects such as microcracks or voids. In this case, the internal defects must be small compared to the representative volume element over which damage is considered. In case of ductile failure, when the propagation of a macrocrack is associated with the nucleation of defects (voids) ahead of crack tip in a so-called fracture process zone (FPZ), damage mechanics has been used to describe the macrocrack propagation itself. There is so far no evidence of such ductile failure in ice. Consequently, we use in the present work damage mechanics to deal with the effect of a field of crevasses on ice flow, and not to describe the propagation of an individual crevasse. Here, as stated by Lemaitre et al. (1988), we consider that CDM describes the evolution of phenomena in the medium from a virgin state to the initiation of macroscopic fractures. In this approach the material is always considered as a continuous material, even when the level of damage is very high. Slow deformation is typically encountered in glaciology, when ice flows slowly under its own weight following the surface slope. CDM has been successfully used in ice-flow models to deal with some glaciological problems such as the flow acceleration of large damaged areas or the opening of crevasses in hanging glaciers (Xiao and Jordaan, 1996; Pralong et al., 2003; Pralong and Funk, 2005; Jouvet et al., 2011; Borstad et al., 2012).

The principle of CDM models is based on the use of a damage variable, usually denoted  $D$ , which represents the degradation of mechanical properties (stiffness, viscosity,...) resulting from a population of defects which effect is averaged at a mesoscale. When considering an anisotropic approach, damage must be represented as a second order tensor (Murakami and Ohno, 1981; Pralong and Funk, 2005). However, following Pralong and Funk (2005), we here consider isotropic damage as a first approximation. In this case, the state variable  $D$  is a scalar quantity, which varies between 0 and 1. While the ice is considered undamaged for  $D = 0$ , full damage is attainable with  $D$  approaching 1.

To describe the effect of damage on the ice flow, an effective **deviatoric** part of the Cauchy stress tensor is introduced:

$$\tilde{\mathbf{S}} = \frac{\mathbf{S}}{(1 - D)}, \quad (8)$$

This effective stress can be understood as the original force applied on an effective undamaged area only. Using the equivalence principle of Lemaitre et al. (1988), strain is affected by the damage only through the effect of an effective stress entering the constitutive equation (see Eq. 3) at the place of  $\mathbf{S}$ , and thus change the expression of the Cauchy stress tensor  $\boldsymbol{\sigma}$  in the Stokes equations (See Eq. 1). Thereby, there is no need to define an effective strain rate.

Our approach deals with a modelling of the viscoplastic flow of ice. The viscous behaviour of the ice is described using Glen's flow law, which links the deviatoric part of the Cauchy stress tensor to the strain rate tensor. Consequently, when accounting only for viscous deformation, damage of the ice only impacts the deviatoric part of the Cauchy stress tensor, and not the cryostatic pressure.

### 2.2.1 Damage evolution

Damage is a property of the material at the mesoscale. It is therefore advected by the ice flow, and evolves through time depending on the stress field. To take this evolution into account, we prescribe an advection equation reading:

$$\frac{\partial D}{\partial t} + \mathbf{u} \cdot \nabla D = \begin{cases} f(\chi) & \text{if } f(\chi) > 0 \\ 0 & \text{otherwise} \end{cases} \quad (9)$$

where the right hand side represents a damage source term  $f(\chi)$ . This term can be written as a function of a damage criterion  $\chi$  and a numerical parameter  $B$ , which we will henceforth call *damage enhancement factor*:

$$f(\chi) = B \cdot \chi \quad (10)$$

In Sect. 3, some sensitivity experiments of the CDM model to the damage enhancement factor are presented.

The choice of the damage criterion is pivotal for the representation of damage increase, and its physical expression is a critical step in the formulation of a CDM model. Commonly used criteria are the Coulomb criterion (Vaughan, 1993), the von Mises criterion (Albrecht and Lev-  
 5 ermann, 2012), or the Hayhurst criterion (Pralong and Funk, 2005; Duddu and Waisman, 2013, 2012). However, these criteria are not necessarily applicable to the damage of ice: the Coulomb criterion is used for a representation of frictional process under compressive loading (*e.g.* Weiss and Schulson, 2009). **The von Mises criterion is a plasticity criterion, aimed at describing the plastic yielding of ductile materials. Hence, it is expressed in terms of deviatoric stresses only, is independent of cryostatic “pressure” (either positive or negative), and symmetric in tension and compression. For all these reasons, it is not suited to describe ice fracturing processes. The Hayhurst criterion (Hayhurst, 1972; Gagliardini et al., 2013a), which involves the maximum principal stress, the cryostatic pressure, and the Von Mises stress invariant, was designed to describe creep damage in ductile materials, and it allows damage under uniaxial compression. Consequently, we think that it is not suited to describe crevasse opening under tension.**

Here, we adopt a pure-tensile criterion, described as a function of the maximum principal  
 15 Cauchy stress  $\sigma_I$ . This choice is consistent with the fact that we want to describe crevasse opening under pure traction, **and is supported by Rist et al. (1999) who argued that crevasses tend to open normal to the direction of maximum tensile stress.** This criterion would also be able to represent a broad variety of crevasses observed on glaciers, such as splaying crevasses.  
 20 Anyway, the implementation of another criterion in the model would be straightforward, and would be an interesting parameter to investigate for future work. The criterion reads as follow:

$$\chi(\sigma_I, \sigma_{th}, D) = \max\left\{0, \frac{\sigma_I}{(1-D)} - \sigma_{th}\right\} \quad (11)$$

Here  $\sigma_{th}$  represents a stress threshold for damage initiation. The corresponding envelope of the damage criterion is represented in the space of Mohr circle in figure. 1.

[Fig. 1 about here.]

The stress threshold for damage initiation  $\sigma_{th}$  corresponds to the overload which must be applied in order to reach the ice strength and initiate degradation. To account for sub-grid scale

heterogeneity, we introduce some noise on  $\sigma_{th}$  :  $\sigma_{th} = \overline{\sigma_{th}} \pm \delta\sigma_{th}$ , where  $\frac{\delta\sigma_{th}}{\overline{\sigma_{th}}}$  follows a standard normal distribution with a standard deviation of 0.05.  $\overline{\sigma_{th}}$  is the mean stress threshold, and usually reaches several tens of kilo-Pascals (Pralong and Funk, 2005). To avoid negative values for  $\sigma_{th}$  arising from the sub-grid scale heterogeneity, the lower bound  $\sigma_{th} > 0$  is prescribed.

5 Sensitivity of the model to this parameter will be discussed in Sect. 3.

This formulation of the damage criterion implies some limitations to the calving model. In particular, it does not account for shear and compressive failure mechanisms. However, it remains consistent with the approach of Benn et al. (2007b), who stated that it is the longitudinal stretching associated to longitudinal velocity gradients which exert a first order control on the development of crevasses in glaciers. Moreover, it is consistent with the fracture mechanics approach explained in Sect. 2.3 which considers crevasses opening in pure tension only.

### 2.2.2 Viscosity modification

As pointed by Pralong et al. (2003) and Pralong and Funk (2005) on alpine hanging glaciers, the ice flow is altered by the accumulation of micro-defects in the ice: damage softens the ice and accelerates the creep. This softening is taken into account through the introduction of the effective stress within Glen's law.

When introducing the effective deviatoric stress tensor  $\tilde{\mathbf{S}}$  and taking into account the equivalence principle, as described in Sect. 2.2, Eq. (3) reads :

$$\tilde{\mathbf{S}} = (A)^{-1/n} \mathbf{I}_{\dot{\epsilon}_2}^{(1-n)/n} \dot{\epsilon} \quad (12)$$

20 When combined with Eq. (8), it becomes:

$$\mathbf{S} = (A)^{-1/n} (1 - D) \mathbf{I}_{\dot{\epsilon}_2}^{(1-n)/n} \dot{\epsilon} \quad (13)$$

By identification with Eq. (3), one can link the enhancement factor E with the damage D, such as

$$E = \frac{1}{(1 - D)^n} \quad (14)$$

For undamaged ice (meaning  $D = 0$ ),  $E = 1$ , the flow regime is unchanged. When the damage increases ( $D > 0$ ),  $E > 1$ , the viscosity of the ice is reduced, and so the velocity of the flow increases. This formulation of the enhancement factor is consistent with the expected behaviour, and it has already been used in previous studies, such as Borstad et al. (2012). The damage then evolves under the effect of the stress field, where the ice undergoes **a critical tensile stress  $\sigma_{th}$  in the direction of the principal stress**, and it exerts a positive feedback on the velocity field.

## 2.3 Fracture Mechanics

Continuum damage mechanics is a reliable tool to deal with the degradation of ice viscosity with increasing damage over long timescales. It can be understood as a way to simulate sub-critical crevasse nucleation and propagation (Weiss, 2004) at a mesoscale, and its role on creep enhancement. However, calving events are triggered by rapid propagation of preexisting fractures, at very short timescales and speeds reaching a significant fraction of the speed of sound. Thus, this process cannot be represented by a viscous rheology (Weiss, 2004). Instead, at such short timescales, the medium should be considered as elastic. In these conditions, Linear Elastic Fracture Mechanics (LEFM) provides a useful tool to account for these features and matches well with the observations done on crevasse depths (Mottram and Benn, 2009). The application of LEFM on the penetration of surface crevasses, originally introduced by Smith (1976), was used by several authors since (Rist et al., 1999; van der Veen, 1998a,b; Nath and Vaughan, 2003). Here, a LEFM model is combined with the damage model previously described to achieve the formulation of a calving law taking into account fast and slow processes controlling glacier fracturing. In LEFM, three modes of crack propagation can be considered: Mode I, Mode II and Mode III, which respectively refer to opening, sliding and tearing. In the following, only the opening mode (Mode I) is considered.

### 2.3.1 LEFM theory

The key physical parameter of LEFM is the stress intensity factor  $K$ . van der Veen (1998a) proposed an expression for  $K_I$  in an idealized case where the opening stress is constant in the

vertical direction. For the considered opening mode I, in the coordinate system  $(x, y, z)$ ,  $K_I$  reads:

$$K_I = \beta \sigma_{xx} \sqrt{\pi d} \quad (15)$$

where  $\sigma_{xx}$  is the horizontal component of the Cauchy stress tensor,  $d$  is the crevasse depth and  $\beta$  is a parameter depending on the geometry of the problem. The crack is considered to propagate vertically. In the ideal case introduced by van der Veen (1998a), fracture propagation was a function of the difference between the opening deviatoric stress  $S_{xx}$ , resulting from horizontal velocity gradients, and the cryostatic pressure (*creep closure*)  $\sigma_p = \rho_i g z$ , corresponding to the weight of the ice, thus,  $\sigma_{xx} = S_{xx} + \rho_i g z$ .

However, when considering real cases, the opening term  $S_{xx}$  (and so  $\sigma_{xx}$ ) is not constant over depth  $z$  or lateral coordinate  $y$ . Consequently, the appropriate formula to calculate the stress intensity factor for an arbitrary stress profile  $\sigma_{xx}(y, z)$  applied to the crack is given by the weight functions method (Labbens et al., 1974):

$$K_I = \int_{y=y_l}^{y=y_r} \int_{z=0}^{z=d} \beta(z, d, H) \sigma_{xx}(y, z) dy dz \quad (16)$$

where  $y_l - y_r$  refers to the glacier width (see Fig. 2). This formula **relies** on the use of the superposition principle: in the case of linear elasticity, the value of the stress intensity factor at the tip of the crack can be seen as the sum of contributions of all individuals point loads along the crack length. In our case, instead of considering the value of the along-flow component of the deviatoric stress tensor at the tip of the crack, we multiplied it by the weight function  $\beta(z, d, H)$  at each vertical coordinate and integrated it over the initial crevasse depth (Labbens et al., 1974). In this way, the effect of an arbitrary stress profile on the stress intensity factor can be taken into account.

[Fig. 2 about here.]

In LEFM theory, a fracture is able to propagate downward in the ice if the stress intensity factor is higher than the fracture toughness  $K_{Ic}$ . The toughness is a property of the material

and strongly depends on the ice porosity. Several experiments have been carried out to relate the value of  $K_{Ic}$  to the porosity (Fischer et al., 1995; Rist et al., 1996; Schulson and Duval, 2009). Inferred values range from  $0.1 \text{ MPa}\cdot\text{m}^{1/2}$  to  $0.4 \text{ MPa}\cdot\text{m}^{1/2}$ . In our calving model, we adopt a constant value of  $0.2 \text{ MPa}\cdot\text{m}^{1/2}$ . The model sensitivity to this value will be discussed in Sect. 3.3.4.

The weight function  $\beta(z, d, H)$  depends on the geometry of the crevasse, and so it depends on the considered problem. Among the weight functions for various crack and **notched** geometries, that have been proposed, we use the one corresponding to an edge crack in an infinitely wide plane plate (Glinka, 1996). A complete description of the weight function and an illustration of the geometry is given in Fig. 2 and Appendix A.

### 2.3.2 Critical damage contour and fracture initiation

From Eq. (16), it is easily understandable that an initiation of crevasse propagation requires a combination of both sufficient tensile stress and large enough initial crevasse depth to exceed fracture toughness. In our model, the size of pre-existing flaws is dictated by a contour of critical damage on the near-surface of the glacier, where damage reaches a critical value  $D_c$ . For application to the LEFM theory, we consider that the depth of this damaged layer corresponds to the initial crevasse depth  $d$  (see Fig. 3). One must keep in mind that this value of  $D_c$  is another threshold which needs to be set. The sensitivity of the model to this parameter will be tested in Sect. 3.

[Fig. 3 about here.]

Compared to the work of van der Veen (1998a,b), we do not consider the presence of water-filled crevasses for the initiation of crack propagation, nor the formation of basal crevasses. **These questions are briefly addressed in Sect. 2.4.** Without these features, **however**, our model is sufficient to provide a lower bound for crevasse propagation.

### 2.3.3 Fracture Arrest

Once the conditions for fracture initiation are fulfilled, we consider that the crevasse propagates vertically. In van der Veen (1998b), crevasses propagate downward as long as the inequation  $K_I \geq K_{Ic}$  is satisfied, thus assuming that  $K_I = K_{Ic}$  represents both a crack propagation and a crack arrest criterion. Such arrest criterion is probably misleading, as the stress intensity factor at arrest, though non-zero, is always lower than the stress intensity factor at propagation (Ravi-Chandar and Knauss, 1984), mostly as dynamical effects have to be taken into account for the arrest condition. Therefore, following Ravi-Chandar and Knauss (1984), we use a crevasse arrest criterion:  $K_I < K_{Ia}$ , with  $K_{Ia} = \alpha K_{Ic}$  and  $0 < \alpha < 1$ . The value of  $\alpha$  for ice is unknown. In the following, we arbitrarily set  $\alpha$  to 0.5. Sensitivity to this value will be discussed in Sect. 3.3.4.

In this simplified LFM framework, calving would theoretically occur only if  $K_I$  remains larger than  $K_{Ia}$  down to the bottom of the glacier. However, as a result of the cryostatic pressure and hydrostatic pressure,  $K_I$  becomes negative before reaching  $d = H$ . To overcome this inconsistency, authors have proposed alternative criteria. Benn et al. (2007a) proposed a first-order approach considering that calving of the aerial part of the glacier occurs when a surface crevasse reaches the sea-level. This criterion is supported by two observations. Firstly, Motyka (1997) showed that calving of the aerial part occurs when the crevasse reaches the sea level, usually followed by the calving of the subaqueous part. Secondly, a surface crevasse reaching sea level may be filled with water, if a connection exists to the open sea (Benn et al., 2007b). In this case, the crevasse will propagate further downward. Indeed, the water adds a supplementary pressure  $\rho_w g d_w$ , where  $d_w$  represents the height of water in the crevasse, equal to the height between the sea level and the crack tip. This supplementary hydrostatic pressure, added to the tensile opening stress, counterbalances the cryostatic pressure and/or the ocean water back pressure. Consequently, the opening full stress  $S_{xx}^*$  dominates the force balance and one expects the crevasse to propagate downward. We performed the calculation of  $K_I$  in the case where a crevasse reaching sea level becomes water-filled. The resulting stress intensity factor becomes positive (up to one kilometer upstream from the front) over the entire glacier depth,

thus supporting Benn's criterion. This parametrization was successfully applied by Nick et al. (2010) on an idealized geometry, and we choose to prescribe the same criterion. Thereby, the stress intensity factor is computed at a depth  $d_f$  equals to the sea level. If  $K_I|_{d_f} \geq K_{Ia}$ , the calving occurs.

5 This framework has two consequences. Firstly, the stress profile  $\sigma_{x'x'}$  used to calculate  $K_I|_{d_f}$  for the arrest criterion is estimated before the propagation of the crevasse. This propagation modifies  $\sigma_{x'x'}$ , but this effect is not considered here. Secondly, if the condition  $K_I|_d \geq K_{Ic}$  is fulfilled but not  $K_I|_{d_f} \geq K_{Ia}$ , nothing happens in the model whereas one would expect some brittle crevasse propagation down to  $d_f$  to occur. In other words, our model considers LEFM to  
10 describe calving but not to simulate crevasse propagation upstream of the calving front.

The calving model described in the previous sections is summarized in Fig. 4.

[Fig. 4 about here.]

The CDM and LEFM models have been implemented in the finite element ice sheet / ice flow model Elmer/Ice. More information regarding Elmer/Ice can be found in Gagliardini et al.  
15 (2013b). A specific improvement of the model was done by incorporating an automatic remeshing procedure when a calving event occurs. The mesh is rescaled, and the variables are interpolated onto the new geometry. The corresponding method is described in Todd and Christoffersen (2014)'s supplementary material. Adittionnally, we implemented an horizontal interpolation for the damage and the stress field, allowing calving to occurs between nodes, thus reducing the  
20 horizontal mesh dependency.

## 2.4 Possible further improvements

### 2.4.1 Water-filled crevasses

25 Among all the improvements which may be added to the model, the presence of surface melt water in crevasses is the most obvious. It has a major effect on their propagation, as it adds a

supplementary hydrostatic force in the stress balance tending to favor crevasse opening. van der Veen (1998b) showed that a water-filled crevasse is able to propagate the whole thickness of the glacier, and trigger calving, as soon as its water-level remains higher than about 10 – 20 m below the surface.

5 The implementation of this feature in our modelling framework is straightforward. To do so, we just have to add a water pressure term in the expression of the Cauchy stress tensor, depending on the water level in the crevasse  $d_w$ , reading:

$$\begin{cases} \sigma'_{xx}(y, z) = \sigma_{xx}(y, z) & \text{if } z > d_w \\ \sigma'_{xx}(y, z) = \sigma_{xx}(y, z) + \rho_w g(d_w - z) & \text{if } z < d_w \end{cases} \quad (17)$$

Then, the stress intensity factor is computed following Eq. 16, using  $\sigma'_{xx}(y, z)$  instead of  $\sigma_{xx}(y, z)$ .

10 However, adding this feature requires the knowledge of the water depth in the crevasse, or the rate of water input, which are currently poorly constrained and difficult to measure.

### 2.4.2 Basal crevasses

15 At the current stage of development, the model does not include the representation of basal crevasses. These latter are invoked as a possible explanation for the production of large tabular icebergs, as they require a full-thickness fracture penetration. This basal propagation is only possible if the glacier is near or at flotation, such that the tensile stress is large enough to initiate fracture opening (van der Veen, 1998a).

20 Nick et al. (2010) included basal crevasses in a physically-based calving law, by adding the pressure of water filling crevasses in the estimate of the penetration length. Once the penetration of top and basal crevasses covers the full thickness of the glacier, calving occurs. In our experiments, we did not notice a sufficient tensile stress in order to generate damage at the base of the glacier, and some work is currently undertaken to study this process. Technically, capturing the fracture propagation at the base of the glacier relies in integrating the effect from the water  
25 pressure at glacier base, reading:

$$\sigma_w(z) = \rho_w g(H_p - z), \quad (18)$$

with  $H_p$  the piezometric head, which represent “the height above the base to which water in a borehole to the bed will rise” (van der Veen, 1998a). But this implementation requires knowledge regarding the value of  $H_p$ , which is difficult to estimate if the glacier is grounded. Considering  $H_p = sl$  could be considered as a reliable upper bound in the vicinity of the front. At the present state, however, our framework still propose a lower bound for calving event size and front retreat.

### 2.4.3 Crevasse shielding

Considering the case of highly crevassed glacier surfaces and closely-spaced crevasses, our fracture propagation framework could not rely on a parametrization, which only consider lone crevasse propagation. In this case, problems arise from the fact that the stress concentrations at crevasse tips are reduced by the presence of neighbouring crevasses (*shielding effect*). The consequence is that it would become harder for a crevasse to propagate downward under the same stress condition. van der Veen (1998b) proposed a parametrization, which could be a potential improvement of our model. In case of a constant tensile stress profile  $S_{xx}$ , the stress intensity factor is modified as a function of the distance between neighboring crevasses  $l$  and the crevasse depth  $d$ , and reads:

$$K_I|_{shielding} = D(L)S_{xx}\sqrt{(\pi dL)}, \quad (19)$$

$$L = \frac{l}{l+d}, \quad (20)$$

where  $S_{xx}$  is the tensile stress, and  $D(L)$  is a weight function which depends on  $L$ . However, this kind of parametrization would require an estimation of  $l$ , which cannot be obtained from our modelling framework at the present stage. Once an estimation of  $l$  could be obtained from another mean, the introduction of such shielding effect in Eq. (16) would be straightforward.

The major effect which could arise from this development would be a supplementary delay in the time and the position of calving events, probably resulting in calving events occurring

nearer to the calving front, where the tensile stress is higher, and as such resulting in smaller size distribution of icebergs.

### 3 A case study

The model is applied to Helheim Glacier, a fast flowing well-monitored glacier in South-East Greenland. The abundance of observations there allows to confront and constrain our model parameters against the past glacier evolution. For our model development, we focus on a two-dimensional flowline problem.

#### 3.1 Data Sources

As stated by Andresen et al. (2011), Helheim glacier's front position remained within an extent of 8km over the last 80 years. During these decades, the glacier showed multiple advances and retreats. In particular, Helheim underwent a strong retreat between 2001 and 2005, before creating a floating tongue which readvanced between 2005 and 2006 (Howat et al., 2007). In the last decade, it has been intensively surveyed and studied (Luckman et al., 2006; Joughin et al., 2008b; Nick et al., 2009; Bevan et al., 2012; Cook, 2012; Bassis and Jacobs, 2013), and therefore constitutes an interesting **case study to calibrate** a calving model.

As we focus on the front evolution and the calving representation, we only need a bedrock topography covering the last kilometers, in the vicinity of the front. For this reason, we choose to follow the work by Nick et al. (2009) and use their dataset in which the last 15 kilometers of the glacier are well represented. In this dataset, the initial front position corresponds to the May 2001 pre-collapse geometry. In addition, we choose to consider the glacier as isothermal near the ice front, prescribing a constant temperature of  $-4.6^{\circ}\text{C}$  (following Nick et al., 2009). **It can be noted here that the constant negative temperature may be inconsistent with the calving criterion, as it will freeze any water in crevasses, and thus will prevent the glacier from establishing a hydraulic connection with the proglacial-water body. However, this constant value was chosen in order to produce a velocity field consistent with the observations, and, for sake of simplicity,**

we did not take into account the vertical variations of temperature. A constant surface mass balance  $a_s$  is taken from Cook (2012) who fitted direct observations from stakes placed over the glacier between 2007 and 2008, which are assumed to represent the annual surface mass balance.

## 5 3.2 Flowline specifications and numerics

Following our notation system, the ice flows along the horizontal “x-direction” and the “z-direction” is the vertical axis.

The geometry covers the last 30 km of the glacier, with an initial thickness varying between 900 m at the inlet boundary, and 700 m at the front. Using the metric from Nick et al. (2009), the beginning of the mesh is located at kilometer 319, and the front at kilometer 347 (see Fig. 5). This geometry is discretized through a structured mesh of 10500 quadrilateral elements, refined on the upper surface and at the front. The element size decreases from 150 m to 33 m approaching the front in the horizontal direction, and from 3.3 m to 68.0 m from top to bottom. Sensitivity tests have been carried out to optimize the mesh size in the vertical direction, and glacier behaviour appears to converge with increasing refinement, such as only negligible difference appears when refining more than 3.3 m at top surface. Thus, our choice allows for a proper fracture initiation and damage advection, as well as a relatively fast serial computation. We employed an Arbitrary Lagrangian Eulerian (ALE) method to account for ice advection and mesh deformation, with a time step of 0.125 day. Sensitivity to the time step size was also undertaken. Below the chosen value, no more significant difference appears in the glacier behaviour, as well as in the calving event size and frequency.

[Fig. 5 about here.]

The specific boundary conditions adopted for the 2D application are described below, with the boundary conditions presented in Sect. 2.1.2 :

The basal friction  $C$  is inferred from the 2001 surface velocity data presented in Howat et al. (2007).

For melting at the calving front, we prescribe an ablation function, linearly increasing with depth, from zero at sea level to  $1 \text{ m day}^{-1}$  at depth. This constant melting parametrization is inspired from the work of Rignot et al. (2010) on four West Greenland glaciers.

The inflow boundary condition ( $x = 319 \text{ km}$ ) does not coincide with the ice divide. As we only consider the last kilometers near the terminus, we assume that ice velocity is constant at the upstream boundary, and we impose a vertically-constant velocity profile of  $u_x = 4000 \text{ m a}^{-1}$ , in agreement with the observed surface velocity from Howat et al. (2007). **However, this is not the case for the inlet flux, which may vary, following the possible evolution of inlet boundary thickness.**

When dealing with a 2D flowline representation of the ice flow, we have to take into account some three-dimensional effects. Especially, lateral friction along the rocky-margins of the glacier can play a significant role, by adding a resistive stress to the flow. Here, we modify the gravitational force using a lateral friction coefficient  $k$ , as proposed by Gagliardini et al. (2010).

$$k = \frac{(n+1)^{1/n}}{W^{\frac{n+1}{n}} (2A)^{1/n}} \quad (21)$$

This coefficient depends on the Glen's flow law parameters  $A$  and  $n$ , as well as on the channel width  $W$ , which is taken from Nick et al. (2009). **The lateral friction coefficient is applied over the whole glacier length, and covers the entire lateral ice surface. It does not account for the tributary glacier, which merges the principal stream near the center of the flow segment.**

Even if the velocity and the surface topography are known and correspond to the observed state of the glacier in May 2001, some relaxation is necessary in order to obtain a stable steady state (Gillet-Chaulet et al., 2012). We let the geometry adjust to the prescribed boundary conditions and inversed basal friction for 8 years.

### 3.3 Results and discussion

#### 3.3.1 Model calibration: sampling strategy

The model is calibrated by varying the three parameters  $\sigma_{th}$ ,  $B$ , and  $D_c$  in a given range. In order to distinguish the effect arising from different damage parameters, we use a Latin Hypercube Sampling (LHS) method with 16 distinct parameters combination for  $(\sigma_{th}, B)$ , that we reproduced for three values of  $D_c$ .

The stress threshold  $\sigma_{th}$  is estimated to lie in range of  $[0.01, 0.20]$  MPa. The lower bound is near to the one given in Pralong and Funk (2005). If  $\sigma_{th} > 0.20$  MPa, the modeled stresses are not high enough to reach the damage threshold, and damaging, when existing, is too weak.

The damage enhancement factor  $B$  was chosen within  $[0.5, 2.0]$ . The explanation for this wide range is the following: when the damage criterion  $\chi$  is positive, the corresponding damage increase releases the stress level in the ice. In reality, this process is happening continuously, such that the stress level cannot exceed the edge of the envelope defined in green line in Fig. 1. However, as our model deals with a finite time step size, the stress level may jump in the “damaging” area (grey-shaded area in Fig. 1). The role of damaging is then to “push” the stress back on the edge of the envelope: the rate of this stress displacement is set by the value of  $B$ . Ultimately, this parameter should be set such that the stress is displaced right on the edge of the damaging envelope. However, this value is difficult to evaluate, especially because stress relaxation occurs through non-linear viscous flow.

The critical damage value  $D_c$  has already been inferred in several studies (Pralong and Funk, 2005; Borstad et al., 2012; Duddu and Waisman, 2013). Following these studies, we used three values of  $D_c$  (0.4 ; 0.5 ; 0.6).

#### 3.3.2 Model calibration: spin-up

Damage can be produced anywhere in the glacier. As we need to obtain a steady state for the damage field, it is necessary to let the damage created upstream be advected to the front. The model is therefore spun-up for 8 years: the front is kept fix at its initial position, without

submarine frontal melting, nor the calving procedure. After 8 years, the front is released, while frontal melting and calving procedure are activated.

### 3.3.3 Model response

Over the last century, Helheim Glacier has probably undergone several advance and retreat cycles (Andresen et al., 2011). The observations of sand deposits show that terminus variation did not exceed 10 km. The knowledge of the potential trigger mechanisms for these cycles is still poor: according to Joughin et al. (2008b) and Andresen et al. (2011), the recent retreat may have been caused by higher summer air and ocean temperature. Yet, the role of the calving activity under these changes remains unclear. For these reasons, we do not try to reproduce the precise chronology of the Helheim's most recent retreat. Instead, we study the dynamical behaviour of the model with respect to the different sets of parameters, and try to distinguish between unrealistic and realistic behaviours. **To distinguish different model behaviour, simulations were run for 10 years using the parameter sets.** The model response can then be split in 3 classes, illustrated in Fig. 6. The first class of model behaviour corresponds to the case where the calving does not happen often. The glacier advances too far and builds up a floating tongue of several kilometers (blue line, Fig. 6). The second class illustrates a case which prolific calving, leading to a front retreat far upstream (yellow line). The last range of behaviour is consistent with observations, where the terminus is punctuated by regular or irregular calving events, forcing the glacier to keep its extent in an acceptable range of values (red line).

[Fig. 6 about here.]

This threefold classification of glacier behaviour can be generalized to the 48 simulations. In order to eliminate aberrant behaviour, we set a sanity-check, by considering plausible sets of parameters as the ones which lead to a simulated front position within the range [340 km, 350 km]. The results are presented in Fig. 7, in the parameter space  $(B, \overline{\sigma_{th}}, D_c)$ . We distinguish again the three classes, blue **triangles**, yellow **circles** and red diamonds, representing respectively the case where the front exceeds 350 km, the case where the front retreats below 340 km, and the case where the front remains within this range.

[Fig. 7 about here.]

The **steady** advance of the front without or with few calving events (**blue triangles**) can be explained considering the parameters  $(B, \overline{\sigma_{th}})$  **as a first approach**. These underlying simulations are characterized by a low value of  $B$  and/or a high value of  $\overline{\sigma_{th}}$ . This means that either the incrementation of damage is too low, or the stress threshold is too high to allow damage initiation. In these cases, damage production may be not sufficient to reach the calving criterion  $D = D_c$ . In addition, when  $\overline{\sigma_{th}}$  is too high, the damage may only increases in the area where the traction is very high, meaning at the top of bumps, in the immediate vicinity of the surface. As a consequence, the damage does never reach a sufficient depth to trigger calving.

On the contrary, the too fast retreat of the front (**yellow circles**) can be explained as follows: when  $B$  is high and/or  $\overline{\sigma_{th}}$  is low, the initiation of damage is easy, and increments quickly, leading to a high damage at the glacier surface. As a consequence, the criterion  $D > D_c$  can be more easily reached, leading to a too rapid sequence of calving events.

**The chosen range for  $\sigma_{th}$  produces acceptable results. When related to the tensile strength of snow and ice, it agrees with constraints from previous studies, especially Borstad (2011) who inferred the tensile strength of snow and firn at the surface to be in the range of 10-50 kPa. Vaughan (1993) found values in the range of 100-400 kPa in the vicinity of crevasses, which is slightly larger than our range. However, deeper knowledge of the firn density at Helheim surface could probably help constraining this parameter further.**

At last, parameter  $D_c$  is a control on whether the fracture propagates. If it is low, the conditions for crevasse propagation are easily reached (as soon as the criterion on LEFM is fulfilled). If  $D_c$  is too high, damage may never reach a sufficient depth to initiate fracture propagation (See Fig. 7). As a consequence, this value controls the location of the calving front. However, it is tightly linked with  $(B, \overline{\sigma_{th}})$  through the production of damage upstream and it must be chosen in the same range as the level of damage at the front.

Nevertheless, the discretization into three classes of parameter should not hide the fact that there is a continuum in the behavior of the glacier, depending on the value of  $(\overline{\sigma_{th}}, B, D_c)$ , and the boundaries between classes are not abrupt. Thus, simulations may present some front

position out of the range [340 km, 350 km] (and then considered as unrealistic), but still have a general dynamics which is not far from realistic behaviours (e.g. yellow curve on Fig. 6).

### 3.3.4 Realistic behaviour

The acceptable parameter combinations are lying on the 3D diagonal described with red diamonds in Fig. 7. During these simulations, the front remained between the two limits and has a consistent behaviour when compared to observations. The simulation corresponding to the parameter set  $\overline{\sigma_{th}} = 0.11$  MPa,  $B = 1.30$  MPa<sup>-1</sup>, and  $D_c = 0.50$  (red star in Fig. 7), can be seen as an example of consistent behaviour. As represented in Fig. 8a,b, damage increases in the area where the traction is high enough to exceed  $\sigma_{th}$ , mostly over bumps. This is consistent with observations of glaciers flowing over slope ruptures (Pralong and Funk, 2005). In these regions, the damage develops up to a depth of almost 15 m, at a rate high enough to reach the critical damage value  $D_c$  at the front and initiate calving (see Fig. 8c and Fig. 8d).

[Fig. 8 about here.]

Mottram and Benn (2009) investigated crevasse depth in the vicinity of the terminus of an icelandic freshwater calving glacier, and showed that most crevasses were no deeper than 10 m. In our model experiment, damage reaches depths of 5 m to 15 m before calving occurs. As described previously, this value of  $d$  must be large enough to account for critical crevasse propagation, and is consistent with observations.

Focusing on this parameter set, we highlight the following main features of the glacier front dynamics. First, at short timescales, the calving activity can be described through a small sizes / high frequency events distribution. This activity is characterized by quasi-periodic front retreats of limited extent (between 50 m and 150 m), associated with a period varying from about 3 to 15 days (down to 1 day for very fast front retreat, see Sect. 3.3.5). These features can be seen in the inset in Fig. 6). Additionally, some outliers (calving events larger than 500 m) also punctuate the front dynamics from time to time.

The front glacier dynamics is also characterized by a larger amplitude / lower frequency oscillation (see Fig. 6), with a period of  $\sim 500/600$  days and a 500 m amplitude. This asymmetric

5 cycle exhibits a slow advance and a quicker retreat, mostly due to a rapid succession of calving events (and not related to the outliers). Despite the complex interactions and feedbacks between damage parameters and ice flow, we can suggest an explanation for these features. Damage reduces ice viscosity, fastens the ice flow, and adjusts glacier geometry. This softening also reduces the stress level as well as the rate of damaging. Additionally, the damage is advected until it reaches conditions where crevasse propagation can trigger calving events (probably because of bending stresses at the front, or processes referred to as second-order processes in Benn et al., 2007b). This calving event results in an immediate increase of the tensile stress in the vicinity of the front (due to force imbalance at the new ice cliff). The subsequent increase of damage 10 where the geometry readjusts may trigger a “cascade” of calving events leading to an important (cumulative) retreat of the glacier front over a limited time scale (a few days / weeks), until the front moves back to a position where the damage is too low to initiate calving. Repeating this process several times leads to the calving cycles highlighted in Fig. 6.

To investigate the strength of this feature, we ran this simulation (red curve in Fig. 6) eight 15 times, using only different local disorder realizations. The Fourier spectrum of the terminus position (Fast Fourier Transform visible in Fig. 9) exhibits a low frequency peak for a period (500 ~ 600 days) approximately equal to the time that ice needs to be advected between the two main bumps visible in Fig. 8, which is likely related to the “cascade” mechanism described above. This feature remains for different parameters sets ( $B$ ,  $\sigma_{th}$ ,  $D_c$ ) (not shown). In Fig. 9, 20 one can also see the smooth and large peak around 3-15 days characterizing the high frequency calving events.

[Fig. 9 about here.]

This observation, combined with the mechanism proposed above, could possibly explain the cycles in front position, and also suggests that the surface geometry (driven by the bedrock 25 topography) exert a control on the calving dynamics, by modifying the rate at which damage primarily develops in the ice. Thus, in the experiments presented in this paper, the slow cycles which can be observed in Fig. 6 are not related to any variability in the external forcing (which remain constant), but result from the **internal glacier dynamics**. This brings us to the conclusion

that a variation of the front position of several kilometers is not necessarily the consequence of an external forcing, **though they might well be triggered by it.**

### 3.3.5 Sensitivity analysis

The analysis proposed in the previous section for one parameters set can be extended to the 12 simulations which successfully passed the sanity check, and this shows that the model's response remain qualitatively unchanged when changing damage parameters. Altogether, we identified 6534 distinct calving events. Characteristics calving event sizes emerge from the distribution, similar to those visible in the inset in Fig. 6, which are illustrated in Fig. 10.

When applied on Helheim Glacier, Cook et al. (2014)'s model furnished a mean calving event size of 450 m, with a frequency of around 14 days. On Store Glacier, for the same zero-forcing conditions, Todd and Christoffersen (2014) obtained a mean size of 80 m, and a frequency of around 8 days. Thus, our 50-150 m range and our 3-15 days period is within the range of these two modelling studies.

[Fig. 10 about here.]

However, one has to remember that this plot should not be interpreted as an icebergs size distribution. Indeed, one must distinguish between the front retreat and the size of resulting iceberg(s), which may be strongly different, as the calved portion of ice can fragment into many icebergs and/or capsizes. However, distribution of the distance of front retreat may remain an interesting parameter to **calibrate** the model, but it would require a continuous tracking of the front position of the actual glacier, as discrete determination of the position (Joughin et al., 2008b) may bias the estimation of the retreat of single events, particularly for the small sizes population. We are not aware of the existence of such a dataset existing on Helheim glacier.

Additionally, the influence of other parameters discussed above was also undertaken. Results shows that the model is only slightly sensitive to the parameter  $K_{Ic}$ . As ice toughness increases, it becomes more and more difficult to initiate fracture propagation. However, changing the value of ice toughness does not change the general behaviour of the system. Varying  $\alpha$  does not have a significant impact. Indeed, the computation of the arrest criterion is realized at depth equals

to the sea level. At this depth, the stress intensity factor is larger than the ice toughness (not shown), and thus, higher than  $K_{Ia}$ , whatever the value of  $\alpha$ .

Finally, the sensitivity to the initial heterogeneous micro-defects distribution introduced in Sect. 2.2.1 was tested. The standard deviation of the distribution of stress threshold  $\frac{\delta\sigma_{th}}{\sigma_{th}}$  was varied within the range [0.005 ; 0.2]. Results are robust under these changes, though the spatial and temporal variability of the front position is modified (not shown). The higher the standard deviation, the more variable is the front position.

[Table 1 about here.]

## 4 Conclusions

In this work, we combined continuum damage mechanics and linear elastic fracture mechanics to propose a physically-based calving model. This model is able to reproduce the slow development of small fractures leading to the apparition of macroscopic crevasse fields, over long timescales, while considering ice as a viscous material. It also allows for the elastic behaviour of breaking ice, consistent with the critical crevasse propagation triggering calving events, characterized by **very short timescales**. The model has been applied to Helheim Glacier, which allowed to constrain **the parameter space for the most important free parameters. Within these constraints, the simulated ice front shows cyclic calving events, while the glacier front stays within the range position observed over the last century.**

The three decisive parameters are the damage initiation threshold  $\sigma_{th}$ , the effect of damage on the viscosity, quantified by the enhancement factor  $B$ , and the critical damage variable  $D_c$ . The first two parameters must be in a range which allows a sufficient damaging upstream before reaching the front by advection. Then, the maximal value of damage should be close to  $D_c$  up to a certain depth in order to trigger calving.

One must keep in mind that this sensitivity test is based on the response of one specific glacier to a poorly known external forcing and with limited observations. Under these conditions, we show that some sets of parameters definitely produce a **reasonable** behaviour, but one should

not readily transfer these to another configuration without consideration, and make sure that the response of the model is realistic. Despite this limitation, this calving model based on realistic physical approaches gives reliable results and could be easily implemented in classical ice-flow models.

5 The calving process described in this paper is immediately driven by the variation in longitudinal stretching associated with horizontal velocity gradients, producing a first-order control on calving rate, as stated by Benn et al. (2007b). Local aspects, involving undercutting or force imbalance at ice cliffs are described as second-order calving processes. Using this model, further work could be undertaken in enhancing the general knowledge of these second-order phenomena.  
10 na.

## Appendix A

### Weight function for stress intensity factor

As stated by Glinka (1996), the weight function for the computation of the stress intensity factor depends on the specific geometry of the initial crack. For an edge crack in a finite width plate,  
15 the weight function is given by:

$$\beta(y, d) = \frac{2}{\sqrt{2\pi(d-y)}} \left[ 1 + M_1 \left(1 - \frac{y}{d}\right)^{1/2} + M_2 \left(1 - \frac{y}{d}\right)^1 + M_3 \left(1 - \frac{y}{d}\right)^{3/2} \right]$$

The weight function depends on 3 numerical parameters, polynomial functions of the ratio  $d/H$ . They read:

$$M_1 = 0.0719768 - 1.513476 \left(\frac{d}{H}\right) - 61.1001 \left(\frac{d}{H}\right)^2 + 1554.95 \left(\frac{d}{H}\right)^3 \\ - 14583.8 \left(\frac{d}{H}\right)^4 + 71590.7 \left(\frac{d}{H}\right)^5 - 205384 \left(\frac{d}{H}\right)^6 + 356469 \left(\frac{d}{H}\right)^7 \\ - 368270 \left(\frac{d}{H}\right)^8 + 208233 \left(\frac{d}{H}\right)^9 - 49544 \left(\frac{d}{H}\right)^{10}$$

$$M_2 = 0.246984 + 6.47583 \left(\frac{d}{H}\right) + 176.456 \left(\frac{d}{H}\right)^2 - 4058.76 \left(\frac{d}{H}\right)^3 \\ + 37303.8 \left(\frac{d}{H}\right)^4 - 181755 \left(\frac{d}{H}\right)^5 + 520551 \left(\frac{d}{H}\right)^6 - 904370 \left(\frac{d}{H}\right)^7 \\ + 936863 \left(\frac{d}{H}\right)^8 - 531940 \left(\frac{d}{H}\right)^9 + 127291 \left(\frac{d}{H}\right)^{10}$$

$$M_3 = 0.529659 - 22.3235 \left(\frac{d}{H}\right) + 532.074 \left(\frac{d}{H}\right)^2 - 5479.53 \left(\frac{d}{H}\right)^3 \\ + 28592.2 \left(\frac{d}{H}\right)^4 - 81388.6 \left(\frac{d}{H}\right)^5 + 128746 \left(\frac{d}{H}\right)^6 - 106246 \left(\frac{d}{H}\right)^7 \\ + 35780.7 \left(\frac{d}{H}\right)^8$$

10 *Acknowledgements.* This study was funded by the Agence Nationale pour la Recherche (ANR) through the SUMER, Blanc SIMI 6 - 2012. We acknowledge the use of data and/or data products from CREsis generated with support from NSF grant ANT-0424589 and NASA grant NNX10AT68G. **We greatly thank Chris Borstad and Jeremy Bassis, whose comments and advice greatly improved the quality of the manuscript. We also thank Doug Benn for pointing out interesting remarks regarding calving state-of-the-art. We further thank the CSC-IT Center for Science Ltd (Finland) for their support in Elmer/Ice development, and Johannes Fürst for helpful thorough reading.**

15

## References

- Albrecht, T. and Levermann, A.: Fracture field for large-scale ice dynamics, *Journal of Glaciology*, 58, 165–177, 2012.
- Andresen, C. S., Straneo, F., Ribergaard, M. H., Bjørk, A. A., Andersen, T. J., Kuijpers, A., Nørgaard-Pedersen, N., Kjær, K. H., Schjøth, F., Weckström, K., and P, A. A.: Rapid response of Helheim Glacier in Greenland to climate variability over the past century, *Nature Geoscience*, 5, 37–41, 2011.
- Åström, J., Riikilä, T., Tallinen, T., Zwinger, T., Benn, D., Moore, J., and Timonen, J.: A particle based simulation model for glacier dynamics, *The Cryosphere*, 7, 1591–1602, 2013.
- Bassis, J. and Jacobs, S.: Diverse calving patterns linked to glacier geometry, *Nature Geoscience*, 6, 833–836, 2013.
- Benn, D. I., Hulton, N. R., and Mottram, R. H.: 'Calving laws', 'sliding laws' and the stability of tidewater glaciers, *Annals of glaciology*, 46, 123–130, 2007a.
- Benn, D. I., Warren, C. R., and Mottram, R. H.: Calving processes and the dynamics of calving glaciers, *Earth-Science Reviews*, 82, 143–179, 2007b.
- Bevan, S. L., Luckman, A. J., and Murray, T.: Glacier dynamics over the last quarter of a century at Helheim, Kangerdlugssuaq and 14 other major Greenland outlet glaciers, *The Cryosphere*, 6, 923–937, 2012.
- Borstad, C. P.: Tensile strength and fracture mechanics of cohesive dry snow related to slab avalanches, Ph.D. thesis, The University of British Columbia, 2011.
- Borstad, C. P., Khazendar, A., Larour, E., Morlighem, M., Rignot, E., Schodlok, M. P., and Seroussi, H.: A damage mechanics assessment of the Larsen B ice shelf prior to collapse: Toward a physically-based calving law, *Geophysical Research Letters*, 39, L18 502, 2012.
- Cook, S., Rutt, I. C., Murray, T., Luckman, A., Zwinger, T., Selmes, N., Goldsack, A., and James, T. D.: Modelling environmental influences on calving at Helheim Glacier in eastern Greenland, *The Cryosphere*, 8, 827–841, 2014.
- Cook, S. J.: Environmental Controls on Calving in Grounded Tidewater Glaciers, Ph.D. thesis, Swansea University, Swansea, United Kingdom, 2012.
- Depoorter, M., Bamber, J., Griggs, J., Lenaerts, J., Ligtenberg, S., van den Broeke, M., and Moholdt, G.: Calving fluxes and basal melt rates of Antarctic ice shelves, *Nature*, 502, 82–92, 2013.
- Duddu, R. and Waisman, H.: A temperature dependent creep damage model for polycrystalline ice, *Mechanics of Materials*, 46, 23–41, 2012.

- Duddu, R. and Waisman, H.: A nonlocal continuum damage mechanics approach to simulation of creep fracture in ice sheets, *Computational Mechanics*, 51, 1–14, 2013.
- Durand, G., Gagliardini, O., De Fleurian, B., Zwinger, T., and Le Meur, E.: Marine ice sheet dynamics: Hysteresis and neutral equilibrium, *Journal of Geophysical Research: Earth Surface* (2003–2012), 114, F03 009, 2009.
- 5 Favier, L., Gagliardini, O., Durand, G., and Zwinger, T.: A three-dimensional full Stokes model of the grounding line dynamics: effect of a pinning point beneath the ice shelf, *The Cryosphere*, 6, 101–112, 2012.
- Fischer, M., Alley, R., and Engelder, T.: Fracture toughness of ice and firn determined from the modified ring test, *Journal of glaciology*, 41, 383–394, 1995.
- 10 Gagliardini, O., Durand, G., Zwinger, T., Hindmarsh, R., and Le Meur, E.: Coupling of ice-shelf melting and buttressing is a key process in ice-sheets dynamics, *Geophysical Research Letters*, 37, L14 501, 2010.
- Gagliardini, O., Weiss, J., Duval, P., and Montagnat, M.: On Duddu and Waisman (2012a,b) concerning continuum damage mechanics applied to crevassing and icebergs calving, *Journal of glaciology*, 59, 797–798, 2013a.
- 15 Gagliardini, O., Zwinger, T., Gillet-Chaulet, F., Durand, G., Favier, L., Fleurian, B. d., Greve, R., Malinen, M., Martín, C., Råback, P., et al.: Capabilities and performance of Elmer/Ice, a new generation ice-sheet model, *Geoscientific Model Development*, 6, 1689–1741, 2013b.
- 20 Gillet-Chaulet, F., Gagliardini, O., Seddik, H., Nodet, M., Durand, G., Ritz, C., Zwinger, T., Greve, R., and Vaughan, D. G.: Greenland Ice Sheet contribution to sea-level rise from a new-generation ice-sheet model, *The Cryosphere*, 6, 1561–1576, 2012.
- Glinka, G.: Development of weight functions and computer integration procedures for calculating stress intensity factors around cracks subjected to complex stress fields, *Stress and Fatigue-Fracture Design*, Petersburg Ontario, Canada, Progress Report, 1, 1, 1996.
- 25 Hayhurst, D.: Creep rupture under multi-axial states of stress, *Journal of the Mechanics and Physics of Solids*, 20, 381–382, 1972.
- Howat, I. M., Joughin, I., and Scambos, T. A.: Rapid changes in ice discharge from Greenland outlet glaciers, *Science*, 315, 1559–1561, 2007.
- 30 Jay-Allemand, M., Gillet-Chaulet, F., Gagliardini, O., Nodet, M., et al.: Investigating changes in basal conditions of Variegated Glacier prior to and during its 1982–1983 surge, *The Cryosphere*, 5, 659–672, 2011.

- Joughin, I., Das, S. B., King, M. A., Smith, B. E., Howat, I. M., and Moon, T.: Seasonal speedup along the western flank of the Greenland Ice Sheet, *Science*, 320, 781–783, 2008a.
- Joughin, I., Howat, I., Alley, R. B., Ekstrom, G., Fahnestock, M., Moon, T., Nettles, M., Truffer, M., and Tsai, V. C.: Ice-front variation and tidewater behavior on Helheim and Kangerdlugssuaq Glaciers, Greenland, *Journal of Geophysical Research: Earth Surface* (2003–2012), 113, F01 004, 2008b.
- Jouvet, G., Picasso, M., Rappaz, J., Huss, M., and Funk, M.: Modelling and Numerical Simulation of the Dynamics of Glaciers Including Local Damage Effects, *Mathematical Modelling of Natural Phenomena*, 6, 263–280, 2011.
- Kachanov, L.: Time of the rupture process under creep conditions, *Isv. Akad. Nauk. SSR. Otd Tekh. Nauk*, 8, 26–31, 1958.
- Labbens, R., Pellissier-Tanon, A., and Heliot, J.: Application de la théorie linéaire de la mécanique de la rupture aux structures métalliques épaisses-Méthodes pratiques de calcul des facteurs d'intensité de contrainte, *Revue de Physique Appliquée*, 9, 587–598, 1974.
- Lemaitre, J., Chaboche, J., and Germain, P.: *Mécanique des matériaux solides*, vol. 7, Dunod Paris, 1988.
- Luckman, A., Murray, T., De Lange, R., and Hanna, E.: Rapid and synchronous ice-dynamic changes in East Greenland, *Geophysical Research Letters*, 33, L03 503, 2006.
- Ma, Y., Gagliardini, O., Ritz, C., Gillet-Chaulet, F., Durand, G., and Montagnat, M.: Enhancement factors for grounded ice and ice shelves inferred from an anisotropic ice-flow model, *Journal of Glaciology*, 56, 805–812, 2010.
- Mottram, R. H. and Benn, D. I.: Testing crevasse-depth models: a field study at Breioamerkurjokull, Iceland, *Journal of Glaciology*, 55, 746–752, 2009.
- Motyka, R.: Deep-water calving at Le Conte Glacier, southeast Alaska, *Byrd Polar Res. Cent. Rep.*, 15, 115–118, 1997.
- Murakami, S. and Ohno, N.: A continuum theory of creep and creep damage, in: *Creep in structures*, pp. 422–444, Springer, Tempaku-cho, Toyohashi, 440, Japan, 1981.
- Nath, P. and Vaughan, D.: Subsurface crevasse formation in glaciers and ice sheets, *Journal of Geophysical Research: Solid Earth* (1978–2012), 108, 2020, 2003.
- Nick, F. M., Vieli, A., Howat, I. M., and Joughin, I.: Large-scale changes in Greenland outlet glacier dynamics triggered at the terminus, *Nature Geoscience*, 2, 110–114, 2009.
- Nick, F. M., van der Veen, C. J., Vieli, A., and Benn, D. I.: A physically based calving model applied to marine outlet glaciers and implications for the glacier dynamics, *Journal of Glaciology*, 56, 781–794, 2010.

- Nick, F. M., Vieli, A., Andersen, M. L., Joughin, I., Payne, A., Edwards, T. L., Pattyn, F., and van de Wal, R. S.: Future sea-level rise from Greenland's main outlet glaciers in a warming climate, *Nature*, 497, 235–238, 2013.
- 5 Nye, J.: The distribution of stress and velocity in glaciers and ice-sheets, *Proceedings of the Royal Society of London. Series A. Mathematical and Physical Sciences*, 239, 113–133, 1957.
- Otero, J., Navarro, F. J., Martin, C., Cuadrado, M. L., and Corcuera, M. I.: A three-dimensional calving model: numerical experiments on Johnsons Glacier, Livingston Island, Antarctica, *Journal of Glaciology*, 56, 200–214, 2010.
- 10 Pralong, A. and Funk, M.: Dynamic damage model of crevasse opening and application to glacier calving, *Journal of Geophysical Research*, 110, B01 309, 2005.
- Pralong, A., Funk, M., and Lüthi, M. P.: A description of crevasse formation using continuum damage mechanics, *Annals of Glaciology*, 37, 77–82, 2003.
- Ravi-Chandar, K. and Knauss, W.: An experimental investigation into dynamic fracture: I. Crack initiation and arrest, *International Journal of Fracture*, 25, 247–262, 1984.
- 15 Rignot, E. and Kanagaratnam, P.: Changes in the velocity structure of the Greenland Ice Sheet, *Science*, 311, 986–990, 2006.
- Rignot, E., Koppes, M., and Velicogna, I.: Rapid submarine melting of the calving faces of West Greenland glaciers, *Nature Geoscience*, 3, 187–191, 2010.
- Rist, M. A., Sammonds, P. R., Murrell, S. A. F., Meredith, P. G., Oerter, H., and Doake, C. S. M.: Experimental fracture and mechanical properties of Antarctic ice preliminary results, *Annals of glaciology*, 23, 284–292, 1996.
- 20 Rist, M. A., Sammonds, P. R., Murrell, S. A. F., Meredith, P. G., Doake, C. S. M., Oerter, H., and Matsuki, K.: Experimental and theoretical fracture mechanics applied to Antarctic ice fracture and surface crevassing, *Journal of Geophysical Research*, 104, PP. 2973–2987, 1999.
- 25 Scambos, T. A., Bohlander, J., Shuman, C., and Skvarca, P.: Glacier acceleration and thinning after ice shelf collapse in the Larsen B embayment, Antarctica, *Geophysical Research Letters*, 31, L18 402, 2004.
- Schulson, E. M. and Duval, P.: *Creep and fracture of ice*, Cambridge University Press Cambridge, 2009.
- Shepherd, A., Ivins, E. R., Geruo, A., Barletta, V. R., Bentley, M. J., Bettadpur, S., Briggs, K. H., Bromwich, D. H., Forsberg, R., Galin, N., Horwath, M., Jacobs, S., Joughin, I., King, M. A., Lenaerts, J. T. M., Li, J., Ligtenberg, S. R. M., Luckman, A., Luthcke, S. B., McMillan, M., Meister, R., Milne, G., Mouginot, J., Muir, A., Nicolas, J. P., Paden, J., Payne, A. J., Pritchard, H., Rignot, E., Rott, H., Sandberg Sørensen, L., Scambos, T. A., Scheuchl, B., Schrama, E. J. O., Smith, B., Sundal, A. V., van

- Angelen, J. H., van de Berg, W. J., van den Broeke, Michiel R. Vaughan, D. G., Velicogna, I., Wahr, J., Whitehouse, P. L., Wingham, D. J., Yi, D., Young, D., and Zwally, H. J.: A reconciled estimate of ice-sheet mass balance, *Science*, 338, 1183–1189, 2012.
- 5 Smith, R. A.: The application of fracture mechanics to the problem of crevasse penetration, *Journal of Glaciology*, 17, 223–228, 1976.
- Todd, J. and Christoffersen, P.: Are seasonal calving dynamics forced by buttressing from ice mélange or undercutting by melting? Outcomes from full-Stokes simulations of Store Gletscher, West Greenland, *The Cryosphere Discuss.*, 8, 3525–3561, <http://www.the-cryosphere-discuss.net/8/3525/2014/tcd-8-3525-2014.html>, 2014.
- 10 van der Veen, C.: Fracture mechanics approach to penetration of bottom crevasses on glaciers, *Cold Regions Science and Technology*, 27, 213–223, 1998a.
- van der Veen, C.: Fracture mechanics approach to penetration of surface crevasses on glaciers, *Cold Regions Science and Technology*, 27, 31–47, 1998b.
- Vaughan, D. G.: Relating the occurrence of crevasses to surface strain rates, *Journal of Glaciology*, 39, 255–266, 1993.
- 15 Weiss, J.: Subcritical crack propagation as a mechanism of crevasse formation and iceberg calving, *Journal of Glaciology*, 50, 109–115, 2004.
- Weiss, J. and Schulson, E. M.: Coulombic faulting from the grain scale to the geophysical scale: lessons from ice, *Journal of Physics D: Applied Physics*, 42, 214 017, 2009.
- 20 Xiao, J. and Jordaan, I.: Application of damage mechanics to ice failure in compression, *Cold Regions Science and Technology*, 24, 305–322, 1996.

**Table 1.** Physical and numerical parameters. Tunable parameters are underlined.

| Parameter                          | Symbol              | Value                               | Unit                                |
|------------------------------------|---------------------|-------------------------------------|-------------------------------------|
| Fluidity parameter                 | $A$                 |                                     | $\text{MPa}^{-3} \text{a}^{-1}$     |
| <u>Damage enhancement factor</u>   | $B$                 | 0.5 to 3                            | $\text{Pa}^{-1}$                    |
| Bed friction parameter             | $C$                 |                                     | $\text{Pa m}^{-1/3} \text{s}^{1/3}$ |
| Crevasse depth                     | $d$                 |                                     | m                                   |
| Water depth inside the crevasse    | $d_w$               |                                     | m                                   |
| Damage variable                    | $D$                 | 0 to 1                              |                                     |
| <u>Critical damage variable</u>    | $D_c$               | 0.4 to 0.6                          |                                     |
| Glen's enhancement factor          | $E$                 | 1                                   |                                     |
| Gravitational acceleration         | $g$                 | 9.81                                | $\text{m s}^{-2}$                   |
| Ice Thickness                      | $H$                 |                                     | m                                   |
| Lateral friction coefficient       | $k$                 |                                     | $\text{Pa m}^{-4/3} \text{a}^{1/3}$ |
| Stress intensity factor (Mode I)   | $K_I$               |                                     | $\text{MPa m}^{1/2}$                |
| Fracture toughness (Mode I)        | $K_{Ic}$            | 0.2                                 | $\text{MPa m}^{1/2}$                |
| Arrest criterion (Mode I)          | $K_{Ia}$            |                                     | $\text{MPa m}^{1/2}$                |
| Sea level                          | $l_w$               |                                     | m                                   |
| Bed friction exponent              | $m$                 | 1/3                                 |                                     |
| Glen exponent                      | $n$                 | 3                                   |                                     |
| Deviatoric stress tensor           | $S$                 |                                     | Pa                                  |
| Effective deviatoric stress tensor | $\tilde{S}$         |                                     | Pa                                  |
| Velocity field                     | $u$                 |                                     | $\text{m s}^{-1}$                   |
| Channel width                      | $W$                 |                                     | m                                   |
| Fracture arrest parameter          | $\alpha$            | 0.5                                 |                                     |
| Weigth function                    | $\beta$             |                                     | $\text{m}^{-1/2}$                   |
| Strain rate                        | $\dot{\epsilon}$    |                                     |                                     |
| Viscosity                          | $\eta$              |                                     | $\text{MPa}^{-1} \text{a}$          |
| Water density                      | $\rho_w$            | 1000                                | $\text{kg m}^{-3}$                  |
| Ice density                        | $\rho_I$            | 900                                 | $\text{kgm}^{-3}$                   |
| Cauchy stress tensor               | $\sigma$            |                                     | Pa                                  |
| Effective Cauchy stress tensor     | $\tilde{\sigma}$    |                                     | Pa                                  |
| Maximum principal stress           | $\sigma_I$          |                                     | Pa                                  |
| <u>Stress threshold</u>            | $\bar{\sigma}_{th}$ | $20 \cdot 10^3$ to $200 \cdot 10^3$ | Pa                                  |

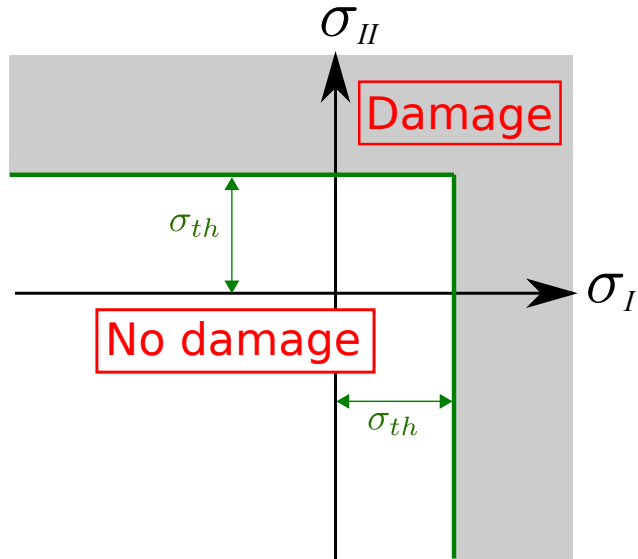


**Fig. 1.** Damage envelope in the space of principal stresses.  $\sigma_I$  and  $\sigma_{II}$  respectively represent the first and the second principal stress, while  $\sigma_{th}$  is the stress threshold. The shaded area corresponds to stress conditions that will cause damaging in the calving model.

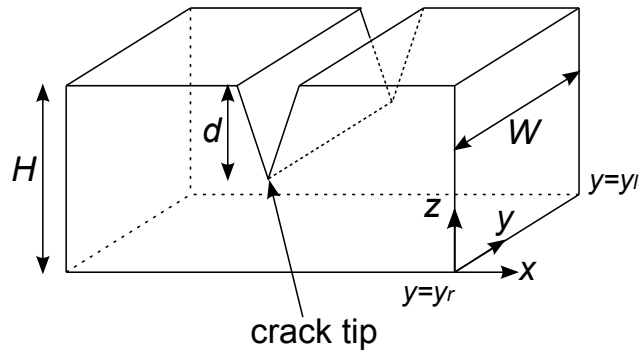


**Fig. 2.** Crevasse shape. See Tab. 1 for parameters list.

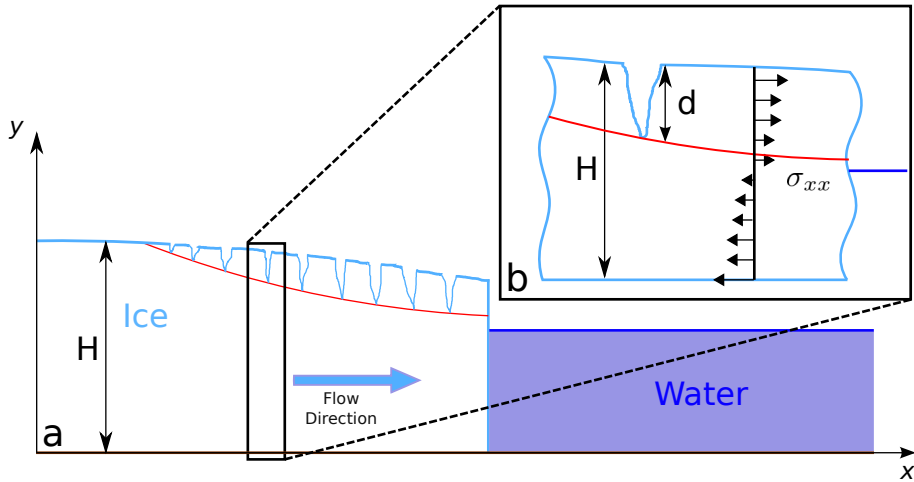


**Fig. 3.** (a) Shape of a grounded glacier and (b) zoom on one crevasse. The red curve illustrates the contour of critical damage  $D = D_c$ , for which we compute the along-flow component of the Cauchy stress tensor  $\sigma_{xx}$  multiplied by the weight function and integrated over the crevasse depth  $d$ .

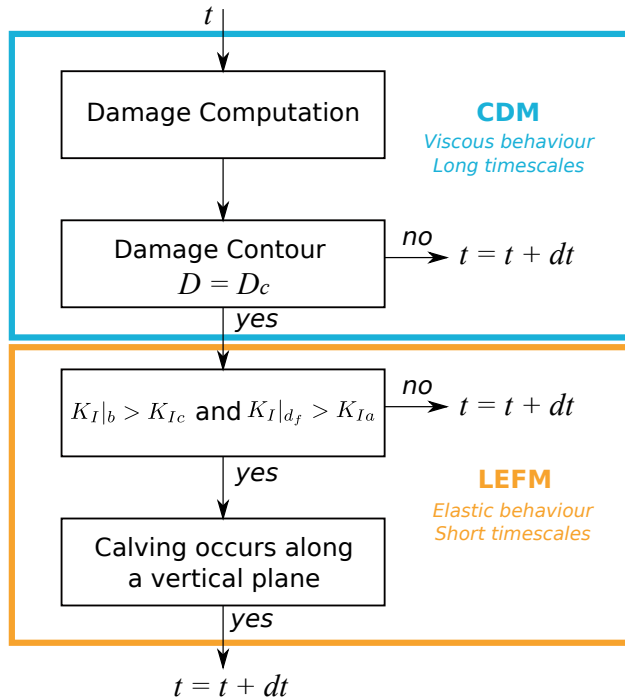


**Fig. 4.** Algorithm of the calving model where  $t$  refers to the time step. Blue shape indicates the area of CDM application, where ice undergoes a viscous behaviour and orange shape corresponds to the LEFM domain of application, where ice has an elastic behaviour, representing fracture propagation and calving event.

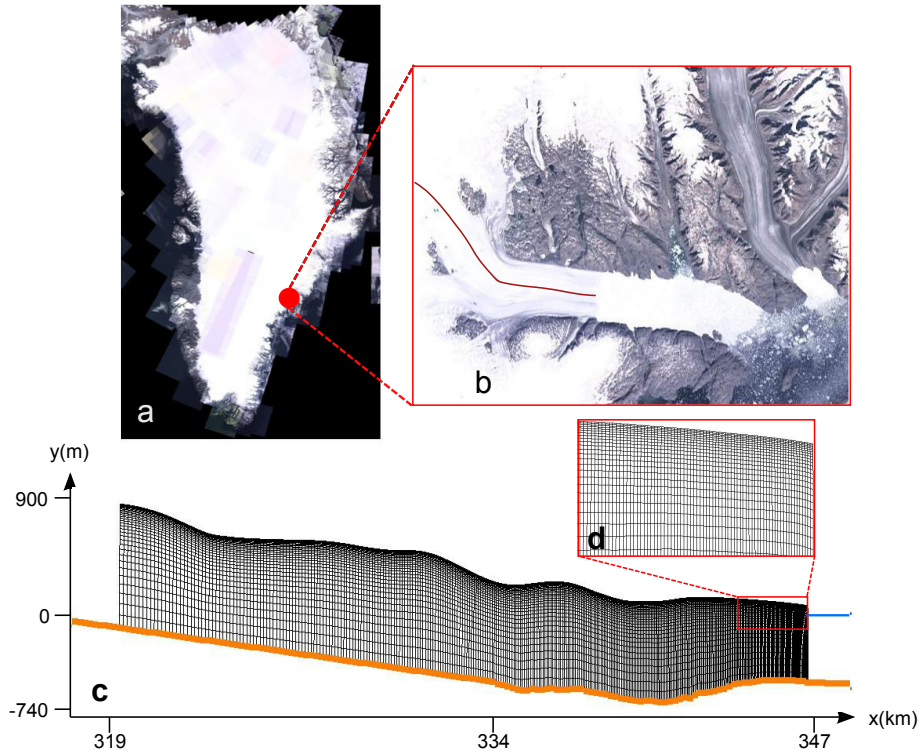


**Fig. 5.** Glacier location and geometry. (a) Location on the Greenland Ice Sheet (red point). (b) Zoom on the Helheim terminus and the considered flowline (red curve). (c) Mesh constructed for this flowline segment. The starting position correspond to the front position at 347km (May 2001). The blue line indicates the sea level. (d) Zoom on the upper surface at calving front.

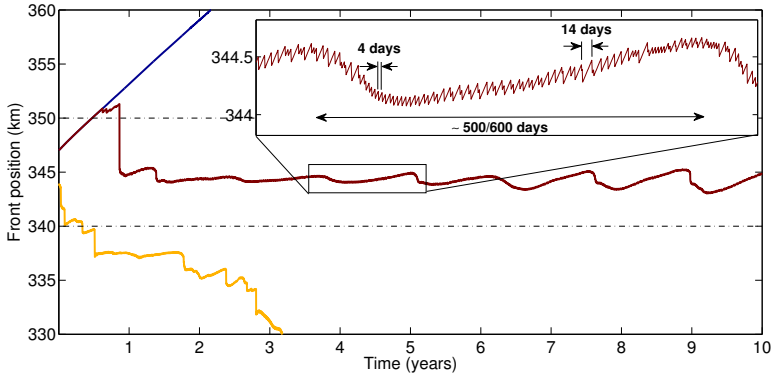


**Fig. 6.** Position of the calving front over ten years. Each color correspond to a set of parameter  $\overline{\sigma_{th}}$ ,  $B$ , and  $D_c$ . The blue color represents an advance with almost no calving ( $\overline{\sigma_{th}} = 0.15$  MPa,  $B = 0.84$  MPa $^{-1}$ , and  $D_c = 0.6$ ); the yellow one corresponds to a severe retreat ( $\overline{\sigma_{th}} = 0.11$  MPa,  $B = 1.30$  MPa $^{-1}$ , and  $D_c = 0.4$ ); the red one presents a behaviour consistent against observations ( $\overline{\sigma_{th}} = 0.10$  MPa,  $B = 1.75$  MPa $^{-1}$ , and  $D_c = 0.50$ ). A zoom of the consistent case is given in the inset.

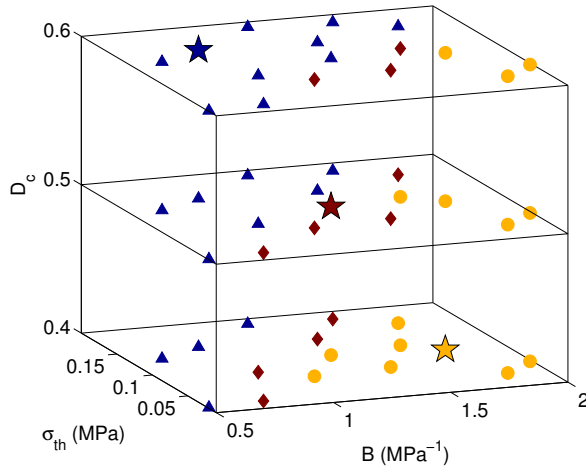


**Fig. 7.** Parameters set for the damage model discriminated by  $B$ ,  $\overline{\sigma_{th}}$ ,  $D_c$ . Blue triangles, and yellow circles respectively represent simulations for which front position exceed 350 km and simulation for which the front retreated below 340 km. Red diamonds are the successful simulations. Colored stars correspond to the three parameters sets illustrated in Fig. 6.

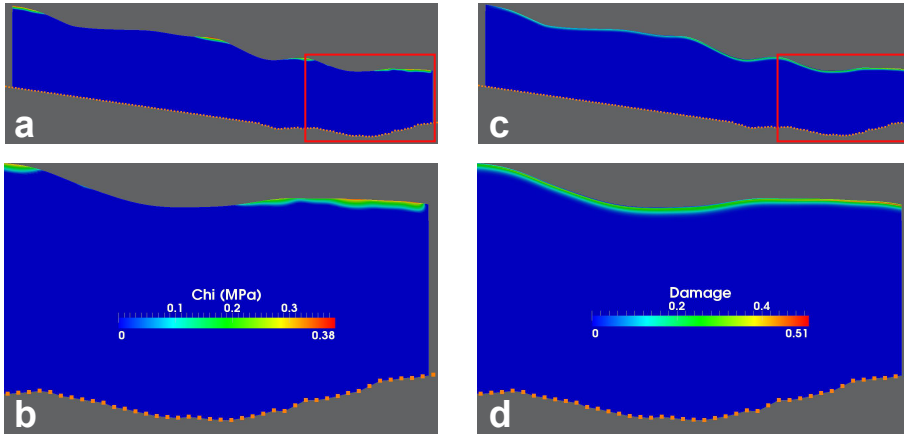


**Fig. 8.** State of Helheim glacier after 365 days of simulation for the set of parameter ( $\overline{\sigma_{th}} = 0.11$  MPa,  $B = 1.30$  MPa $^{-1}$ , and  $D_c = 0.50$ ) corresponding to the red star on Fig. 7.  $\chi$  is the damage criterion, positive where damage will accumulate. (a) Damaging areas of Helheim glacier and (b) zoom on the red rectangle; (c) Damage field and zoom on the red rectangle (d).

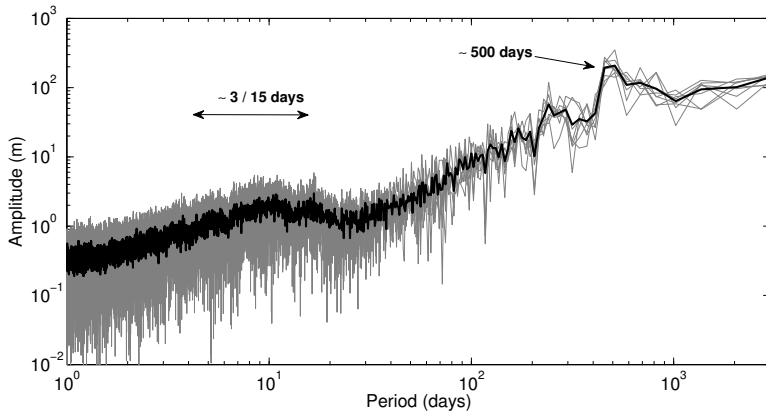


**Fig. 9.** Frequential response of the calving front variations for 8 realizations of the set of parameters ( $\sigma_{th}=0.11\text{MPa}$ ,  $B = 1.30\text{MPa}^{-1}$ ,  $D_c=0.50$ ), computed over 10 years. Grey lines represent the frequency spectrum for each of the eight simulations, and the corresponding mean is drawn in black thick line.

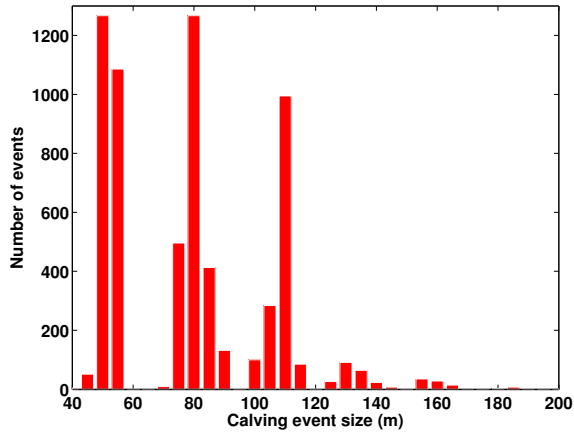


**Fig. 10.** Distribution of the calving events sizes corresponding to the 12 realistic simulations. Different modes can be related to various damage parameters combinations. Calving event size axis is truncated at 200 m. However, a few events, up to 2000 m, were recorded.